Progress In Electromagnetics Research M, Vol. 42, 61–70, 2015

Inter-Subject Variability Evaluation towards a Robust Microwave Sensor for Pneumothorax Diagnosis

Maria Christopoulou* **and Stavros Koulouridis**

Abstract—Pneumothorax is the medical condition caused by the air concentration inside the pleural cavity, the space between the lung and the chest wall. Apart from traditional diagnostic methods, it can be detected by using microwave sensors that capture variations in reflected electromagnetic field (EMF). Sex and obesity, related to the internal composition of the biological tissues, can influence the reflected EMF and therefore the sensor diagnostic ability. This paper investigates the effect on the performance of a proposed on-body dual-patch antenna sensor for pneumothorax diagnosis, due to inter-subject variability in underlying tissue structure. The sensor operates at frequency range of 1–4 GHz. The challenge of the paper is to propose frequency bands for robust and safe sensor operation. S_{12} parameter alternation versus frequency is assessed for healthy and pathological cases. Implemented thorax numerical models include modified (i) closed rectangular multilayered and (ii) MRI-based anatomical ones. In rectangular models, thickness and configuration of muscle, fat and bone tissues are varied, according to literature. Additionally, sex-related anatomical differences are taken into account in MRI-based models. All scenarios are solved using Finite Difference Time Domain method. Results revealed that the proposed frequency bands lie within 1–2.7 and 2.9–3.5 GHz, for muscle, 1.4–3.5 GHz for fat and 1–2.2 and 2.8–3.5 GHz, for bone variations. Numerical evaluations for accurate anatomical models verify the findings.

1. INTRODUCTION

Pneumothorax is the abnormal collection of air or gas in the pleural space that separates the lung from the chest wall. The trapped air presses the lung and affects normal respiration, drastically. Progressive build-up of pressure in the pleural space pushes the mediastinum to the opposite hemithorax and obstructs venous return to the heart. This leads to circulatory instability and may result in traumatic arrest. If pneumothorax is not diagnosed and treated on time, it can cause lung collapse and a life threatening emergency. The reported causes of pneumothorax include: chest injuries during an accident, underlying lung diseases, ruptured air blisters or mechanical ventilation. Pneumothorax is categorized to (i) primary spontaneous, which occurs in healthy people and is not caused by an injury and (ii) secondary, which is related to a pre-existing disease. The overall person consulting rate for pneumothorax (primary and secondary combined) in England reaches 0.24‰ a year for men and 0.1‰ a year for women [1].

Pneumothorax is normally diagnosed using a chest X-ray. Computerized tomography (CT) scan may be also needed to provide more detailed images. However, during emergencies, a portal, low-cost and easy-to-use instrumentation should be available in ambulances. During the last decades, wireless modules for body-worn applications have been developed and applied in the field of microwave

Received 21 February 2015, Accepted 16 April 2015, Scheduled 4 May 2015
* Corresponding author: Maria Christopoulou (mchrist@ece.upatras.gr).
The authors are with Laboratory of Electrotechnics, Department of Electrical and Computer Engineering, University of Patras, Patras 26504, Greece.

healthcare monitoring, facilitating the disease prediction and diagnosis. Microwave imaging utilizes low-power on-body antennas that can describe non-invasively the internal structure of underlying tissues, by monitoring the reflected electromagnetic field. Such applications are reported in plenty medical cases, like mammography [2] and stroke diagnosis [3].

This study presents the performance characteristics of a compact microwave sensor, composed by two low-power patch antennas, for non-invasive and real-time pneumothorax detection [4]. The proposed sensor detects the reflected electromagnetic wave that alters in amplitude and phase due to the underlying trapped air, which differs significantly in dielectric properties from the surrounding biological tissues. The scope of the present work is to reveal the effect of inter-subject variability of the internal anatomical tissue structure on the performance of the proposed microwave sensor, used for pneumothorax diagnosis. Inter-subject variability factors such as gender, weight, height, obesity and fitness level can influence the thickness of the underlying tissues, mainly fat and muscle. The big challenge is to overcome such factors and detect the frequency bands where pneumothorax can be diagnosed safely and independently of the examined patient profile. For this purpose both rectangular layered and MRI-based thorax models are applied. The rest of the paper is structured as following: Section 2 provides the theoretical background of the applied methodology and the numerical models of the dual patch antenna sensor and thorax phantoms. Application scenarios and results are presented and discussed in Section 3, while the paper concludes in Section 4.

2. MATERIALS AND METHODS

2.1. Background for Air Detection Methodology

Assume a homogeneous electromagnetic plane wave propagating in free space on z direction, vertically incident onto a structure of N successive layers of biological tissue:

$$\underline{E}^{inc} = \hat{x} E_0 e^{-jk_0 z} \tag{1}$$

where $k_0 = \omega\sqrt{\varepsilon_0 \mu_0}$ is the wave number for free space, ω the angular frequency, ε_0 the permittivity, and μ_0 the magnetic permeability for free space. The amplitude of the electromagnetic wave reflected by or transmitted through the body depends strongly on the dielectric properties of the tissues. The complex relative permittivity of a biological tissue is expressed by the Cole-Cole equation [5]

$$\dot{\varepsilon}_r(\omega) = \varepsilon_r(\omega) + \frac{\sigma(\omega)}{j\omega\varepsilon_0} \tag{2}$$

where ε_r is the relative permittivity and σ the conductivity. The penetration depth and the wavelength of the electromagnetic wave that propagates into the biological tissue are respectively expressed by:

$$\delta = \sqrt{\frac{2}{\omega\sigma\mu_0}} \tag{3}$$

$$\lambda = \frac{\lambda_0}{\sqrt{\varepsilon_r}} \tag{4}$$

where λ_0 is the free space wavelength. As well known, δ and λ depend on frequency and tissue dielectric properties ε_r and σ. The dominant biological tissues from the skin to the pleural cavity of thorax are: skin, fat, muscle and bone, in case of the ribs. In order to define frequency region of interest, δ and λ are calculated for skin and fat, i.e., tissues that respectively correspond to high and low water-content, at $f = 1$ and 10 GHz. Penetration depth δ varies from 20.7 to 1.8 mm for skin and 71.1 to 5.7 mm for fat, while wavelength λ from 50.1 to 5.7 mm for skin and 134.2 to 15.3 mm for fat. Since the average chest wall thickness (CWT) does not exceed 35 mm [6] and the required sensor's resolution is 5–20 mm [7], the frequency range of 1–4 GHz is considered sufficient for the antenna sensor, as described in detail in [8].

2.2. Dual Patch Antenna Sensor

In order to detect the air layer into the body, a sensor built from two planar patch antennas is applied [4]. Each patch is $1.44 \times 1.44\,\text{cm}^2$. A square ($2.9 \times 2.9\,\text{cm}^2$) dielectric substrate made of Rogers RO3210

(ε_r = 10.2 and $\tan\delta$ = 0.003, thickness = 0.2286 cm) interposes. The patch is fed at 0.5 cm off-center on x-axis by coaxial cable through its substrate. The detailed geometry of the antenna is depicted in Fig. 1(a), while in Fig. 1(b) the corresponding printed patch antenna is shown. In Fig. 1(c) simulated and measured data for reflection coefficient S_{11} in free space are presented. Simulations have been carried out using Finite Difference Time Domain (FDTD) [9] and Finite Element methods (FEM) [10], implemented in the corresponding software platforms: SEMCAD-X 14.8.4 [11] and Ansys HFSS 15.0 [12]. The S_{11} difference in FEM and FDTD results is due to differentiation in feed pin modeling. Measurements have been performed with a Keysight Technologies PNA Vector Analyzer, N5221A 10 MHz–13.5 GHz [13]. Satisfactory agreement is achieved. The maximum shifting in resonant frequency is found between FDTD simulations (2.82 GHz) and measured patch 1 (3.07 GHz). Differences between the two measured patches are due to fabrication issues and are considered minor. Additionally, the far field radiation pattern as computed in HFSS is illustrated in Fig. 1(d) at 3 GHz, for $z > 0$, i.e., above the ground plane. After rigorous investigation [4], the relative antennas' configuration which was proved to be most effective, considering the air detection ability resulted to antennas intermediate separation distance of 2 cm and crossed positioning of the coaxial feeding probe.

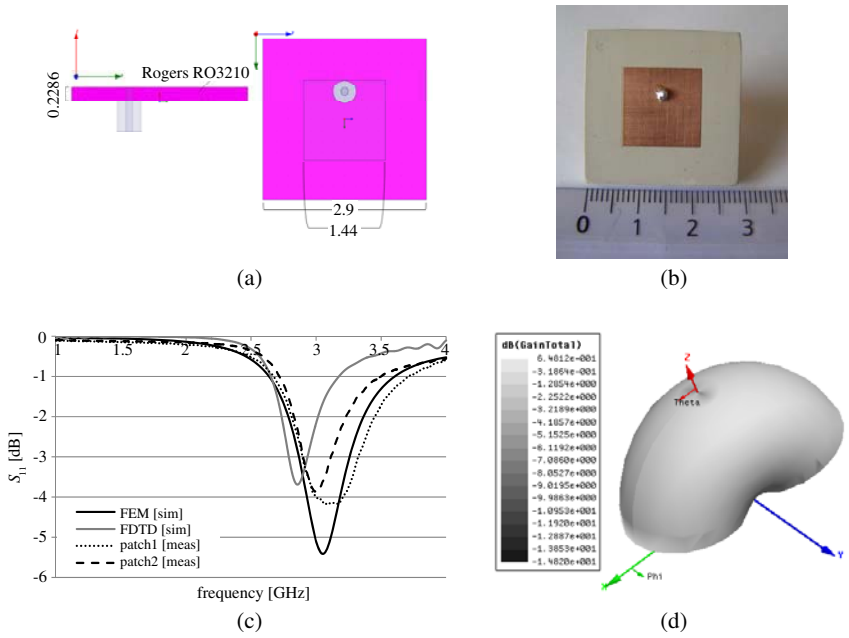

Figure 1. (a) Geometrical details of the patch antenna (dimensions in cm), (b) front face of printed patch antenna on Rogers 3210 substrate, (c) measured and simulated S_{11} variation within the frequency range of 1–4 GHz, for free space operation, (d) antenna far field radiation pattern (gain) for free space operation, at 3 GHz, for $z > 0$.

2.3. Tissue Numerical Models

The healthy and pneumothorax implemented torso are numerically simulated by using rectangular and anatomical models. In detail, the following models are applied:

THORAX: A closed rectangular multilayered thorax numerical model. It consists of dry skin, fat, air and inflated lung, in order to model a typical closed section of the thorax in the intercostal space (no rib present). The dimensions of the model are based on the average values of two anatomical MRI-based Virtual Family whole-body models, Duke and Ella [14]. Duke and Ella correspond to 34-year-old male and 26-year-old female, respectively. Therefore, THORAX model has width (x axis): 324.90 mm, depth (z axis): 200.20 mm while height (y axis) is selected equal to λ_0 free space wavelength at f = 1 GHz (i.e., 300 mm). The surrounding skin layer thickness is set stable to 5 mm at both x and z axes and 0 mm at y axis, representing the thorax cut. The lungs are modeled as box, based again on the averaged

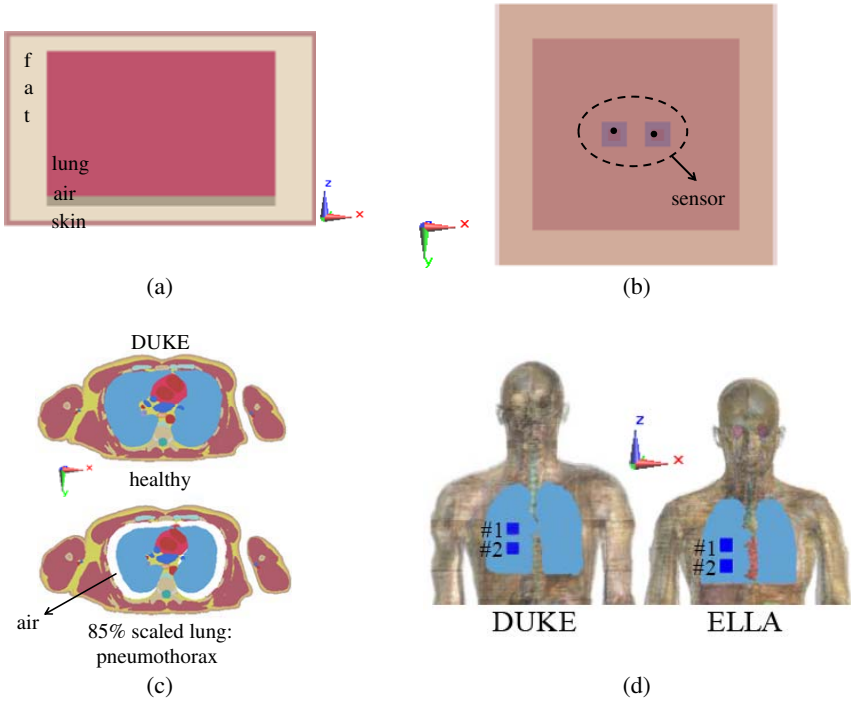

Figure 2. Internal structure of numerical torso model of: (a) THORAX on XZ plane, where skin, air (10 mm layer for pneumothorax modeling), lung and fat tissues are present, (b) relative crossed configuration of the two patch antennas onto the skin surface of THORAX, (c) healthy (top) and pneumothorax (bottom) cases, implemented in DUKE model, illustrated on XY plane, (d) positioning, relatively to the voxelized lungs, of the two (#1 and #2) patch antennas onto the skin surface of DUKE and ELLA.

dimension values of Duke and Ella lungs. Therefore, the lungs have width (x axis): 238.10 mm, depth (z axis): 159.62 mm and height (y axis): 220.42 mm. The rectangular lungs are centered into the THORAX, resulting to fat layer thickness of 38.40 (x axis), 15.29 mm (z axis) and 39.79 mm (y axis). Pneumothorax is modeled by entering 10 mm of air layer between fat and lung tissues. The tissue layers into the THORAX phantom are illustrated in Fig. 2(a). The relative crossed configuration of the two patch antennas onto the skin surface of the THORAX is illustrated in Fig. 2(b).

DUKE and ELLA: A section of the thorax (including lungs) of two anatomical Virtual Family whole-body numerical models, Duke and Ella. The thorax sections DUKE and ELLA have been modified in order to model a typical pneumothorax case. The following approach has been applied: lungs are scaled down to 85% in x (width) and y (depth) axes, resulting to air gap of 1.5–2.0 cm (Fig. 2(c)). The air extent is selected according to British Thoracic Society that defines that distance between the pleural surface and the lung edge of 2 cm or more represents a pneumothorax that occupies at least 50% of the affected hemithorax [7].

3. RESULTS AND DISCUSSION

3.1. Performance of the Dual-Antenna Sensor onto THORAX

The performance of the dual-antenna sensor for the selected configuration is assessed based on differential simulations of the S_{12} variation onto healthy and pathological THORAX. In order to illustrate the sensitivity of the sensor, Figure 3 plots the S_{12} variation onto thorax within 1–4 GHz frequency range for air thickness varying from 0.5 to 2 cm, with 0.5 cm step. It is obvious that the sensor provides satisfactory diagnostic performance from 0.5 cm, enabling the early pneumothorax diagnosis. Moreover, as the air layer becomes thicker, the S_{12} difference increases slightly in the frequency range of interest.

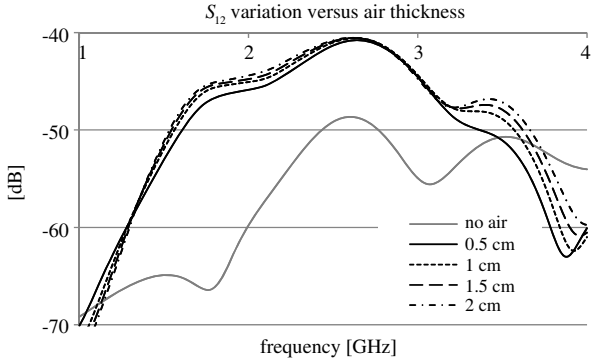

Figure 3. Performance assessment of the dual-antenna sensor by plotting S_{12} variation onto THORAX within 1–4 GHz frequency range for air thickness varying from 0.5 to 2 cm with 0.5 cm step.

In [15] detailed comparison between simulated and measured diagnostic performance for a very similar to THORAX model experimental thoracic phantom is carried out. It is concluded that sensor performance and sensitivity are verified. In following application scenarios, it has been decided to use air thickness of 1 cm, as reference in THORAX model, which corresponds to the half thickness of 2 cm, specified by British Thoracic Society [7] for pneumothorax definition.

3.2. Application Scenarios

In order to evaluate how the internal tissue structure can influence the diagnostic ability of the sensor, the simplified THORAX phantom is used as a reference. The inter-subject and sex structural variability is studied by varying the thickness of muscle, fat and bone layers that interpose between fat and lung (or air in case of pneumothorax). Therefore, apart from the THORAX phantom, the following modified phantoms are assessed: i) *muscle* thickness at 0 (reference: THORAX), 5, 10, 15, 20, 25 mm (6 cases), ii) *fat* layer thickness at 0, 5, 10, 15 (reference: THORAX), 20, 25 and 30 mm (7 cases), iii) *bone* layer thickness at 0 (reference: THORAX), 5, 10, 15 mm and rectangular ribs of 15 mm width with 15 mm intercostal space (6 cases). In the last modeling, the alternation between gap and rib is inverted, in order to change the tissue structure below the two patch antennas. The ribs width and the average intercostal space are both set to 15 mm, which are based on literature [16]. The range of tissue thickness values is based on sex-related data, body regions of examination and inter-subject variability, due to obesity or fitness factors. More specifically, when the sensor is placed onto the chest, the internal tissue structure is mainly composed by muscle in men (more than 20 mm in DUKE) and by breast fat in women (almost 30 mm in ELLA). However, the sensor is expected to be applied onto the anterior second intercostal space (ICS) at the midclavicular line (MCL) and in the lateral forth intercostal space of the affected hemithorax. These two locations are considered the most common regions [17] where the air is trapped during pneumothorax, given the lying position of the patient. These regions are selected due to the minimal thickness of underlying intermediate tissues (fat and muscle) and to the smallest distance to the trapped air.

In all evaluations, healthy (air thickness: 0 cm) and pneumothorax (air thickness: 1 cm) are compared. The dual-antenna sensor is placed onto the skin surface (Fig. 2(b)) of all modified tissue phantoms and the S_{12} coefficient is calculated, assessing its potential differentiation, due to the presence of air close to the lung. Additionally, the two patch antennas (#1 and #2) are placed onto DUKE and ELLA chest (Fig. 2(d)), modeling the worst-case differentiation, due to sex-related anatomic significant difference in fat and muscle composition. Due to skin curvature, the applicator mismatch is corrected by adding water, between skin surface and antennas' patches [4]. Table 1 provides the underlying tissues' thickness in the two XY planes that correspond to the level of each patch feeding.

Tissues are clustered in two categories: a) 'connective tissue+muscle+cartilage' and b) 'fat+breast' in both DUKE and ELLA models, based on similar dielectric properties that characterize each category. Indicatively, at frequency of 2.3 GHz, the dielectric constant of first category's tissues vary between 40 and 53, while for the second category the variation is restricted between 5 and 11. All electromagnetic

Table 1. Tissue thickness (in mm) in two XY planes, corresponding to the level of each patch feeding. Tissues are clustered as 'connective tissue+muscle+cartilage' and 'fat+breast' in both DUKE and ELLA models.

Tissue	DUKE		ELLA	
	plane #1 (mm)	*plane #2 (mm)*	*plane #1 (mm)*	*plane #2 (mm)*
connective tissue+ muscle+cartilage	27	20	13	8
fat+breast$^{\alpha}$	4	5	20	29

a. breast present only in ELLA model

exposure problems are solved by applying Finite Difference Time Domain (FDTD) method, using software platform SEMCAD-X 14.8.4 [11]. Broadband simulations are carried out for frequency range of 1–4 GHz. Multipole Debye materials are selected to characterize electrically the biological tissues [5].

3.3. THORAX: Muscle, Fat and Bone Variation

Figures 4(a)–(f) illustrate the S_{12} variation within 1–4 GHz frequency range, for healthy (red) and pathological (black) cases implemented in THORAX. Muscle (Figs. 4(a)–(b)), fat (Figs. 4(c)–(d)) and bone (Figs. 4(e)–(f)) thickness vary according to selected value ranges. Solid lines define the S_{12} variation range within its minimum and maximum values, while the dashed lines plot the mean frequency-dependent variation for each case. The illustration aims to highlight the frequency band where the two ranges have no overlap and therefore diagnosis is considered safe, since the two cases can be distinguished, despite the differences in the intermediate tissue thickness. Figs. 4(a), (c), (e) illustrate the S_{12} variation for the above mentioned range of tissue thickness. It is obvious that for a wide range of tissue thickness variation, healthy and pathological cases cannot be distinguished, safely. In detail, for muscle thickness from 0 to 25 mm (Fig. 4(a)), there is no frequency band, where the sensor can diagnose pneumothorax with safety. On the contrary, for fat thickness variation between 0 and 30 mm (Fig. 4(c)), and bone between 0 and 15 mm (Fig. 4(e)), S_{12} variation ranges are separated even for a narrow frequency band, which is 1.4–2.3 GHz and 1–2.2 GHz, respectively. If during the patient examination, the sensor is placed onto the side of the affected hemithorax, in between the ribs, avoiding large muscles (e.g., for men: pectoralis major muscle) or fatty regions (e.g., for women: breast), the tissue thickness variation can be restricted to a more realistic range, corresponding to muscle range from 0 to 5 mm (Fig. 4(b)), fat from 0 to 15 mm (THORAX) (Fig. 4(d)) and bone between 0 mm and 15 mm rectangular ribs of different relative configuration to the patch antennas (Fig. 4(f)). Expansion of the above restricted ranges would spoil the sensor diagnostic performance. Now, the two regions are distinguished more easily, enabling the differentiation between pneumothorax and healthy cases. More specifically, muscle variation results to safe case distinction within the frequency bands of 1–2.7 and 2.9–3.5 GHz, fat within the band of 1.4–3.5 GHz and bone within the bands of 1–2.2 and 2.8–3.5 GHz. Last, in order to illustrate the distinction of the mean values variation within 1–4 GHz, the absolute

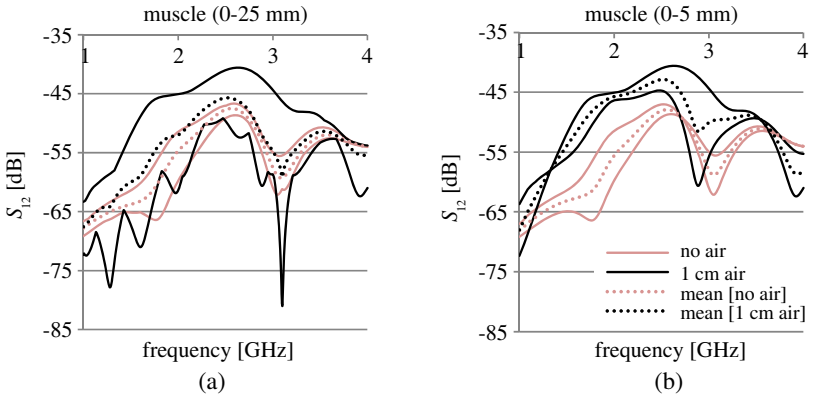

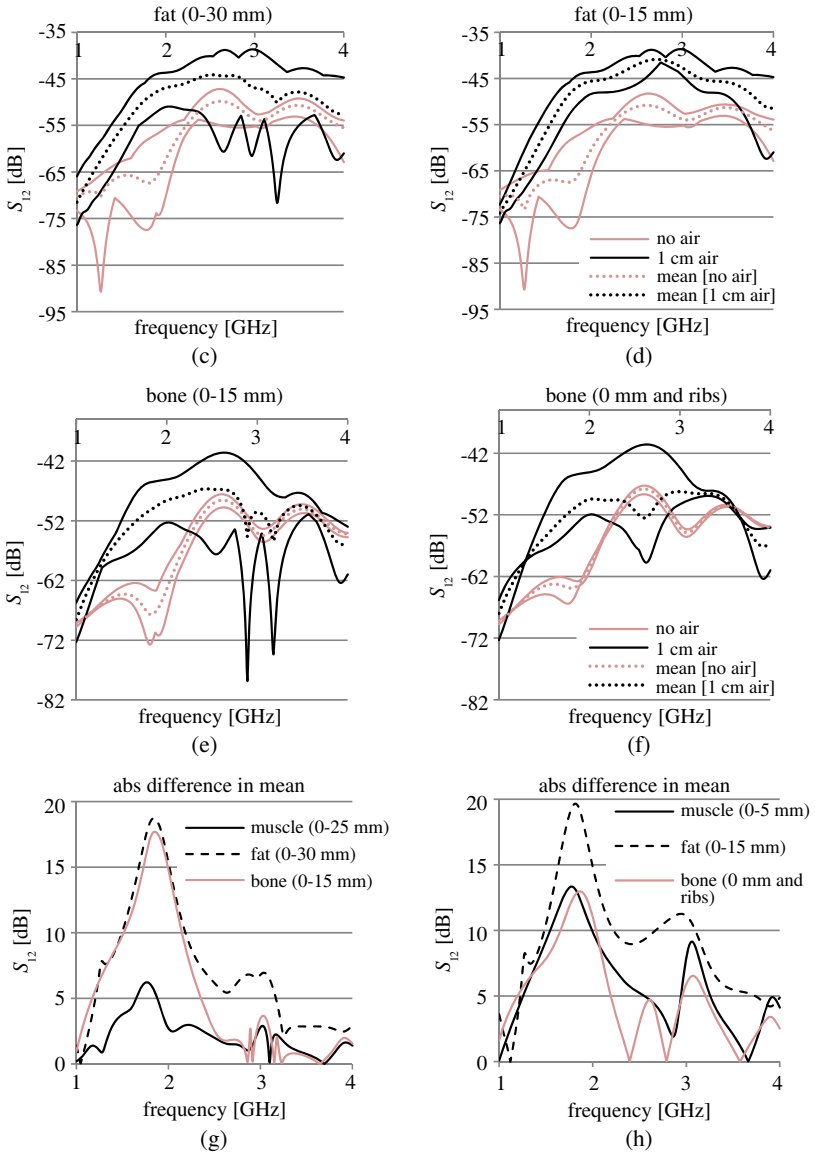

Figure 4. S_{12} variation within the frequency range of 1–4 GHz, for dual patch antenna sensor operating onto THORAX phantom and modified ones, by altering (a)–(b) muscle, (c)–(d) fat and (e)–(f) bone layer thickness. Solid lines correspond to S_{12} variation range (minimum and maximum values), while dashed lines to mean corresponding variation. No overlapping of the two regions indicates safe diagnosis of pneumothorax. Absolute difference in mean variation between healthy and pathological cases, corresponding to the (g) wide and (h) narrow tissue thickness range.

difference in mean variation between healthy and pathological cases is plotted in Figs. 4(g) and (h) corresponding to the wide and narrow tissue thickness range, respectively. It is concluded that for the wide tissue thickness range, the difference in mean values is more than 10 dB within 1.5–2.1 GHz for fat and bone variation while for the narrow range, the difference is more than 10 dB within 1.6–2.0 GHz for muscle and bone and within a wider band (1.5–3.0 GHz) for fat. These findings are verified adequately by the concluded frequency bands where the diagnosis is safe, for each tissue thickness range. However, it should be emphasized that non-overlapping of the extremes (min and max values) of the S_{12} variation range is the safest way to categorize healthy and pathological case, taking into account the tissues thickness variation.

3.4. DUKE and ELLA: Worst-Case Sex-Related Internal Anatomic Structure Variation

As mentioned above, the positioning of the two antennas onto the chest of the realistic models DUKE and ELLA corresponds to representation of the worst-case scenario of the sensor application (Fig. 2(d)). This is due to the relatively large thickness of muscle in DUKE and fat in ELLA. Fig. 5(a) illustrates the thickness and composition of the underlying tissues below the sensor's patch #1 in 'healthy' DUKE and ELLA models. Comparison of the S_{12} variation within the frequency range of 1–4 GHz, between healthy and pneumothorax cases is plotted in Fig. 5(b). The maximum differentiation is located at 2.3 GHz in DUKE and 1.7 GHz in ELLA, reaching 7 dB and 19 dB respectively. These frequencies are within the band of 1.5–2.5 GHz, found for canonical problems, where the safe diagnosis of pneumothorax is enabled, as depicted in Figs. 4(b), (d), (f).

The electric field distribution is also assessed on XY plane, for these frequencies, at the height of patch feed #1, for healthy and pneumothorax case in DUKE (Fig. 5(c)) and ELLA (Fig. 5(d)). Figs. 5(c)–(d) depict the relative volume of the lungs, while the non-uniformity of the electric field distribution is clear due to the existence of the trapped air between the lungs and the chest wall. All values are normalized to 1 W input power, resulting to maximum value of $1.64E+03$ V/m, which corresponds to 0 dB in colorbar. Last, in order to conform to IEEE C95.1-2005 [18] (peak spatial SAR averaged over 10 g of mass, $\text{psSAR}_{10\,\text{g}} < 2$ W/kg) basic restrictions for general public exposure,

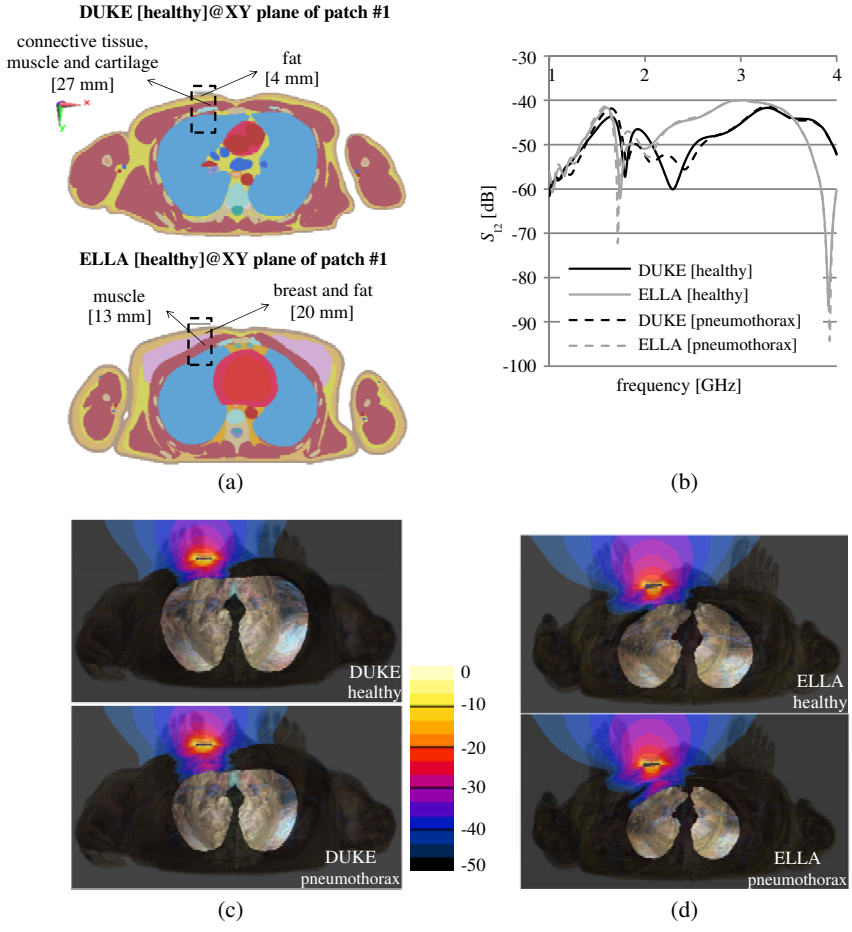

Figure 5. (a) Inner composition and thickness of the patch antenna's underlying tissues in DUKE and ELLA healthy models, (b) S_{12} variation within the frequency range of 1–4 GHz, for dual patch antenna sensor operating onto DUKE and ELLA models with and without air, (c)–(d) E-field distributions on XY plane, at the height of patch feed #1, for healthy and pneumothorax case in (c) DUKE and (d) ELLA. All values are normalized to 1 W input power, resulting to maximum value of $1.64E+03$ V/m.

the actual input power of the patch antenna #1, should not exceed 49 mW, which will result to the maximum value of $\text{psSAR}_{10\,\text{g}}$ (2 W/kg) in DUKE.

4. CONCLUSIONS

This work assesses the performance of a proposed microwave pneumothorax sensor in relation to inter-subject variability in the internal tissue composition. Our contribution is to extract the frequency bands where pneumothorax can be diagnosed independently of the examined patient profile, concluding to a safe and robust sensor. Evaluating muscle, fat and bone thickness in modified planar torso models, the frequency bands lie within 1–2.7 and 2.9–3.5 GHz, for muscle, 1.4–3.5 GHz for fat and 1–2.2 and 2.8–3.5 GHz, for bone. In realistic application scenarios, the worst-case positioning of the sensor onto the chest of anatomical models verifies the findings of the canonical scenarios. More specifically, the frequencies (2.3 GHz in male and 1.7 GHz in female model), for which healthy and pneumothorax cases are clearly distinguished, are located within the band of 1.5–2.5 GHz, where the safe diagnosis of pneumothorax is enabled. In future, the findings will be verified by measurements on customized experimental thorax phantom and by conducting in-vivo experiments on samples of supervised pigs. The described methodology is indented to be tested with broadband antenna sensors, as well.

ACKNOWLEDGMENT

The research project is implemented within the framework of the Action "Supporting Postdoctoral Researchers" of the Operational Program "Education and Lifelong Learning" (Action's Beneficiary: General Secretariat for Research and Technology), and is co-financed by the European Social Fund (ESF) and the Greek State.

REFERENCES

1. Wakai, A. P., "Spontaneous pneumothorax," *Clin Evid*, (Online), pii: 1505, 2011.
2. Conceicao, R. C., M. O'Halloran, M. Glavin, and E. Jones, "Comparison of planar and circular antenna configurations for breast cancer detection using microwave imaging," *Progress In Electromagnetics Research*, Vol. 99, 1–20, 2009.
3. Mohammed, B. J., A. M. Abbosh, D. Ireland, and M. E. Bialkowski, "Compact wideband antenna for microwave imaging of brain," *Progress In Electromagnetics Research C*, Vol. 27, 27–39, 2012.
4. Christopoulou, M. and S. Koulouridis, "Dual patch antenna sensor for pneumothorax diagnosis: Sensitivity and performance study," *Proceedings of IEEE Annual International Conference of the IEEE Engineering in Medicine and Biology Society, IEEE EMBC 2014*, 4827–4830, Chicago, USA, Aug. 2014.
5. Gabriel, S., R. W. Lau, and C. Gabriel, "The dielectric properties of biological tissues: III. Parametric models for the dielectric spectrum of tissues," *Phys. Med. Biol.*, Vol. 41, No. 11, 2231–2293, 1996.
6. Frank, M., V. Schorge, K. Hegenscheid, A. Angermaier, A. Ekkernkamp, N. Hosten, R. Puls, and S. Langner, "Sturdivan's formula revisited: MRI assessment of anterior chest wall thickness for injury risk prediction of blunt ballistic impact trauma," *Forensic. Sci. Int.*, Vol. 212, 110–114, 2011.
7. British Thoracic Society, *Pleural Disease Guidelines*, Sep. 2010.
8. Christopoulou, M. and S. Koulouridis, "Design requirements of microwave sensor for pneumothorax diagnosis," *Proceedings of IEEE International Symposium on AP/URSI*, 2052–2053, Florida, USA, Jul. 2013.
9. Taflove, A. and S. C. Hagness, *Computational Electrodynamics: The Finite-difference Time-domain Method*, 2nd edition, Artech House, 2000.
10. Reddy, J. N., *An Introduction to the Finite Element Method*, 3rd edition, McGraw-Hill, 2005.

11. SEMCAD-X, Schmid & Partner Engineering AG: http://www.speag.com/products/semcad/overview/.
12. Ansys HFSS 15.0: http://www.ansys.com/.
13. Keysight Technologies: http://www.keysight.com/.
14. Christ, A., et al., "The virtual family — Development of surface-based anatomical models of two adults and two children for dosimetric simulations," *Phys. Med. Biol.*, Vol. 55, No. 2, N23–N38, 2010.
15. Christopoulou, M., M. Capstick, B. Reumer, S. Koulouridis, and N. Kuster, "Experimental thorax prototype for multistage pneumothorax diagnosis," *Proceedings of Joint Meeting of The Bioelectromagnetics Society (BEMS) and the European BioElectromagnetics Association (EBEA), BioEM2015*, Asilomar Conference Center, California, USA, Jun. 14–19, 2015.
16. Kim, Y. S., M. J. Park, H. Rhim, M. W. Lee, and H. K. Lim, "Sonographic analysis of the intercostal spaces for the application of high-intensity focused ultrasound therapy to the liver," *Am. J. Roentgenol.*, Vol. 203, No. 1, 201–208, 2014.
17. *Advanced Trauma life Support Program for Doctors*, 6th Edition, American College of Surgeons, Chicago, IL, 1997.
18. IEEE Standard C95.1-2005, *IEEE Standard for Safety Levels with Respect to Human Exposure to Radio Frequency Electromagnetic Fields, 3 kHz to 300 GHz*, 2005.